Uncertainties In Ice Sheet Altimetry From A Space-Borne 1064 nm Single Channel Lidar Due To Undetected Thin Clouds

Yuekui Yang, Alexander Marshak, Tamás Várnai, Warren Wiscombe, and Ping Yang

***Abstract*— In support of the ICESat-II mission, this paper studies the bias in surface elevation measurements caused by undetected thin clouds. The ICESat-II satellite will only have a 1064 nm single channel lidar on board. Less sensitive to clouds than the 532 nm channel, the 1064 nm channel tends to miss thin clouds. Previous studies have demonstrated that scattering by cloud particles increases the photon path length, thus resulting in biases in ice sheet elevation measurements from space-borne lidars. This effect is referred to as atmospheric path delay. This paper complements previous studies in the following ways: First, atmospheric path delay is estimated over the ice sheets based on cloud statistics from the Geoscience Laser Altimeter System (GLAS) on board ICESat and the Moderate Resolution Imaging Spectroradiometer (MODIS) on board Terra and Aqua. Second, the effect of cloud particle size and shape is studied with the state-of-the-art phase functions developed for MODIS cirrus cloud microphysical model. Third, the contribution of various orders of scattering events to the path delay is studied and an analytical model of the first order scattering contribution is developed. This paper focuses on the path delay as a function of telescope FOV. The results show that reducing telescope FOV can significantly reduce the expected path delay. As an example, the average path delays for FOV=167 μrad (a 100 m diameter circle on the surface) caused by thin undetected clouds by the 1064 nm channel over Greenland and East Antarctica are illustrated.**

***Index Terms*— ICESat-II; atmospheric path delay; radiative transfer; polar cloud; lidar altimetry.**

I. Introduction

SPACE-BORNE lidars, such as the Geoscience Laser Altimeter System (GLAS) on board the Ice, Cloud, and land Elevation Satellite (ICESat), provide measurements of ice sheets and sea ice on a global scale. These data are used to address important climate questions, such as "How is the cryosphere responding to the climate change?" and, "How is the change in ice sheets affecting the global sea level?"[1]. To answer these questions, accurate ice surface elevation measurements are needed. The ICESat science objectives require detecting long-term elevation changes with an accuracy of <1.5 cm/year over ice sheet areas of 100x100 km^2 [1] [2].

Atmospheric factors, e.g., clouds, aerosols and atmosphere humidity, may affect the accuracy of the derived ice surface elevation. Among these factors, clouds probably cause the most uncertainty due to the large variability in their properties. Clouds affect lidar measurements through particle forward scattering [3], which increases the photon path length and makes the surface appear farther from the satellite. This effect is referred to as "atmospheric path delay". Some of the pioneering studies on this effect were reported by Duda et al. [2] and Mahesh et al. [4]. These studies demonstrated that the magnitude of the atmospheric path delay is a function of cloud height, cloud optical depth (COD, referred hereafter as τ), cloud particle size and shape, and the telescope field of view (FOV). It was found that the delay could reach tens of cm even for optically thin clouds with a low cloud base.

The challenge in cloud induced atmospheric path delay is two-fold. First, if we know that the lidar beam hits a cloud, how do we correct the retrieved surface elevation? Second, if some clouds are not detected due to the low signal-to-noise ratio of the instrument, how large may the bias be in the altimetry products? Much progress has been made in addressing the first question [2] [4]. The second question is not a pressing issue for ICESat, because the GLAS lidar has two channels, one at 1064 nm and one at 532 nm. The 532 nm channel, used as the primary channel for GLAS atmospheric products, is very sensitive to the presence of clouds [5] [6]. It has been shown that cloud layers with an optical thickness as low as 0.01 generally were detectable with a well-functioning 532 nm laser channel [5]. However, the ICESat-II mission will only have the 1064 nm channel, and undetected clouds will become an important issue. It is critical to understand the probability that the 1064 nm channel may miss the detection of some clouds, and how the missed clouds may affect the altimetry measurements.

Manuscript received April 10, 2009. This work was supported by the National Aeronautics and Space Administration's ICESat II Science Definition Project.

Yuekui Yang is with the Goddard Earth Science and Technology Center, University of Maryland, Baltimore County, Baltimore, MD 21228 USA (phone: 301-614-6313; fax: 301-614-6307; e-mail: yuekui.yang@ nasat.gov).

Alexander Marshak is with the NASA Goddard Space Flight Center, Greenbelt, MD 20771 USA (e-mail: Alexander.marshak@nasa.gov).

Tamás Várnai is with the Joint Center for Earth Systems Technology, University of Maryland, Baltimore County, Baltimore, MD 21228 USA (e-mail: tamas.varnai@nasa.gov)

Warren Wiscombe is with the NASA Goddard Space Flight Center, Greenbelt, MD 20771 USA (e-mail: warren.j.wiscombe@nasa.gov).

Ping Yang is with Department of Atmospheric Sciences, Texas A&M University, College Station, TX 77843 USA (e-mail: pyang@ariel.met.tamu.edu).

The ICESat-II mission is recommended by the National Research Council's Decadal Survey as one of the top priority NASA missions [7]. However, without the 532 nm channel, its ability to detect clouds will be less than that of the current ICESat mission. Following [5], Fig. 1 illustrates this problem. The figure shows the percentage of the undetected clouds by the 1064 nm channel, compared to the cloud detection results by the 532 nm channel. The data are the 1 Hz products from the GLAS campaign conducted from 25 September to 19 November 2003 (termed L2A) [5] [6][8]. As can be seen from the figure, 43% of clouds with an optical depth of 0.1 were undetected by the 1064 nm channel over Greenland, and 29% over East Antarctica. For clouds with an optical depth of 0.2, 27% of clouds over Greenland and 19% over East Antarctica were undetected. Also shown in Fig. 1 is the cumulative cloud fraction, defined as the frequency of occurrence of clouds with optical depth smaller than a certain value out of the total number of observations (cloudy and clear). The cumulative cloud fraction shows how often clouds within certain optical depth range occur. For example, the fraction of clouds with optical depth smaller than 0.2 is 17% over Greenland and 9% over East Antarctica. Calculations show that during the L2A period the total cloud fractions are 60% and 34% over Greenland and East Antarctica, respectively (not shown). It should be pointed out that during the L2A campaign, most of the observations over Greenland and East Antarctica were conducted during nighttime and daytime, respectively. Over Greenland, there was less interference from solar background radiances, and more thin clouds were detected than over East Antarctica.

Using cloud properties observed by GLAS and MODIS, this study will address two main questions in support of the ICESat-II mission: (1) what is the expected delay caused by the undetected clouds as a function of telescope FOV? and, (2) how small the FOV must be to meet the science requirement? The paper is organized as follows. Section II gives a review of how different cloud properties affect atmospheric path delay with a focus on the cloud particle phase function. In Section III, we discuss the contributions of different orders of scattering to the delay. Section IV conducts a cloud detectability comparison between the 532 nm and the 1064 nm channels. Statistics of the properties of the thin clouds that the 1064 nm channel fails to detect are presented in Section V. Section VI estimates the average atmospheric path delay resulting from the undetected clouds. The conclusions of this study are discussed in Section VII. An analytical model for the path delay caused by single scattering is presented in the Appendix.

II. Parameters affecting atmospheric path delay

In this study, simulations are conducted with our 3D radiative transfer Monte Carlo model [9] that has been validated by the International 3D Radiation Code (I3RC) project [10]. Lidar pulses are assumed to be the Dirac-delta function. The shape of the lidar pulse does not affect our results, because atmospheric path delay is calculated as an average value of the delays experienced by individual photons. It should be pointed out that the surface altitude bias is one half of the path delay. In the simulations, clouds are assumed to be horizontally and vertically homogenous. Since we focus on thin clouds over polar ice sheets, the cloud particle phase is presumed to be ice.

Cloud properties, e.g., height, optical depth and particle size and shape, are essential to the determination of atmospheric path delay [2]. Fig. 2 gives some examples of the effect that different parameters have on path delay. Fig. 2a shows atmospheric path delay as a function of the cloud base height for clouds of two different optical depths (0.1 and 0.2) and two FOVs (475 μrad and 167 μrad). 475 μrad, which translates to a 285 m diameter circle on the surface for the 600 km orbital altitude of the satellite, is the FOV of the current ICESat; 167 μrad, which corresponds to a 100 m diameter circle on the surface, is the proposed FOV of ICESat-II [11]. In general, photons scattered by low clouds experience longer paths inside the telescope FOV than the ones scattered by high clouds; hence, path delay generally decreases as cloud base height increases. However, the path delay is not always a monotonic function of cloud base height. Rather, it is a cumulative result of several factors (ref. Appendix), including, phase function, maximum scattering angle and cloud optical depth. It should be noted that the effect of cloud geometrical thickness acts collaboratively with cloud base height. For clouds with the same base height, the thicker the cloud, the higher is the equivalent cloud altitude. Obviously, cloud optical depth is another important factor in the determination of path delay. A larger optical depth means higher probability of photons being scattered, thus causing a larger path delay.

Fig. 2b displays the effect of cloud particle phase functions and telescope FOV on atmospheric path delay. Simulations were conducted for a variety of phase functions, including: the phase function adopted by the MODIS ice cloud property retrievals (see Refs. [12] and [13] for details); the phase functions associated with nonspherical particle shapes such as hollow columns, plates and spheres [13]; and, the isotropic phase function. The results show that particle phase function is an important factor, especially for large FOVs. Moreover, the path delay is essentially a forward scattering issue as can be seen that for the isotropic phase function, the delay is much smaller and practically negligible for FOV < 300 μrad compared to the results from other phase functions. Additionally, the size of the telescope FOV is another important factor that affects path delay determination. The larger the FOV, the higher is the probability of multiple scattered photons reaching the sensor; hence, reducing the FOV could reduce path delay substantially. For example, for the current ICESat FOV (475 μrad), a cloud with an optical depth of 0.2, a base height of 0.5 km and a geometrical thickness of 0.5 km will cause a path delay of about 16 cm (for the MODIS phase function and r_e = 20 μm). However, if the FOV is reduced to 167 μrad, the path delay for the same cloud is reduced to 2.5 cm.

III. Contribution of different orders of scattering

To further understand the mechanism of atmospheric path delay, we separate the results into contributions from different orders of scattering. Fig. 3 shows these contributions, as a function of FOV, for cloud optical depths of 0.05, 0.1 and 0.2. In the figure, the scattering number is the accumulated times that a photon is scattered within a cloud. For example, first order scattering means the photon is only scattered once in the cloud, which can happen either on the downward path to the surface or on the upward path to the sensor. Obviously, the thicker the cloud, the more important is multiple scattering. For the case shown here, if τ = 0.05, the contribution from single order scattering is about 95%; if τ = 0.1, the contribution is about 90%; and, if τ = 0.2, the contribution is about 80%. Generally, for thin clouds, results from first order scattering gives a good approximation to path delay, especially for small FOVs.

The path delay resulting from first order scattering can be calculated analytically. We present the derivation and validation of an analytical model for first order scattering induced path delay in the Appendix. A model that includes second order scattering will be presented in a follow-up study.

Fig. 4a illustrates how the lidar back scattering and path delay are distributed among different orders of scattering for two FOVs, 475 μrad and 167 μrad. Since the cloud is thin (τ = 0.1), the lidar signal is dominated by the non-scattered photons. In this case, about 90% of the lidar returned signal is from non-scattered photons, and about 10% is from photons being scattered once within the cloud. As expected, the plot also shows that for the larger FOV, multiple scattering contributes more to both the backscattering signal and the path delay. Fig. 4b demonstrates the probability of photons being scattered up to a given scattering angle for a variety of particle shapes. As expected from diffraction theory (e.g.,[3]), about 50% of all photons are scattered into a narrow forward-scattering peak.

For first order scattering, the maximum scattering angle for a photon to stay in the FOV can be calculated as (see the Appendix):

$$\theta_s = \arctan\left(\frac{f \times 10^{-6} \times h}{2z}\right) \quad (1)$$

where $h = 6*10^6$ m (satellite orbital height), f is the FOV in μrad and z is the cloud altitude in meters.

For cloud altitudes between 500 m and 6000 m, and for 100 μrad ≤ FOV ≤ 500 μrad, the maximum scattering angle ranges from 0.5° to 15°. The lidar return from zero order scattering and first order scattering can be approximately expressed as: $\frac{1}{1+\tau} \times 100\%$ and $\frac{\tau}{1+\tau} \times 100\%$ (see the Appendix for details). For τ = 0.1, calculations show that photons without any scattering account for 91% of the lidar returns and photons being scattered once account for 9%. These numbers match the Monte Carlo results.

The aforementioned simulations apply only to clouds. Blowing snow is another factor that could potentially cause large path delays over polar ice sheets. Fig. 5 presents path delay calculations using the analytical model given in the Appendix. The optical depth is assumed to be 0.05, so the first order scattering approximation is applicable. As shown in the figure, even a thin layer of blowing snow (τ = 0.05) can ensue a large path delay (over 10 cm for some particle shapes). However, this paper will only focus on path delays resulting from clouds. The effect of blowing snow needs further investigation and will be addressed in our future studies.

IV. Cloud detectability comparison between the 532 nm and the 1064 nm channel

As mentioned in Section I, it is critical for the ICESat-II mission to understand what fraction of thin clouds would be missed by a single 1064 nm channel lidar and what path delay the undetected clouds would cause. To investigate the capability differences in detecting thin clouds between the 532 nm and 1064 nm laser channels, we use the data from the GLAS campaign L2A. As mentioned in Section I, L2A, which is the first GLAS campaign with full on-orbit operation of the instrument, began on 25 September and lasted until 19 November 2003. The GLAS cloud retrievals are archived in the products GLA09, global cloud heights for multi-layer clouds, and GLA11, global thin cloud/aerosol optical depths data [14]. The data used here are the one 1 Hz cloud property retrievals.

Fig. 6 displays the results for Greenland and East Antarctica. East Antarctica and West Antarctica are divided along the traditional boundary, the Transantarctic Mountains [15]. Similar to Fig. 4 in [5], Fig. 6 shows the frequency distribution of GLAS cloud optical depths retrieved using the 532 nm channel observations together with the frequency that the1064 nm channel flagged as cloudy for the corresponding optical depths. In addition, Fig. 6 gives the cumulative distribution of thin clouds missed by the 1064 nm channel, defined as the frequency of missed clouds out of all the transparent clouds detected by the 532 nm channel. Transparent clouds are clouds thin enough for GLAS to have ground return. We see that about 31% of all the transparent clouds were not detected by the 1064 nm channel over Greenland (Fig. 6a) and 22% over East Antarctica (Fig. 6b). Undetected clouds are primarily thin clouds with τ < 0.2. We can see from Fig. 7 that for clouds with τ < 0.2 (Fig. 7a), the difference between cloud detection results of the 1064 nm channel and the 532 nm channel is significant, yet for clouds with τ > 1.0, both channels give similar results (Fig. 7b).

It should be noted that the ability of the 1064 nm channel to detect thin clouds is a function of a variety of factors, such as atmospheric conditions, laser power, and algorithm. In this study, we used the laser on board the current ICESat as a benchmark.

V. Properties of Thin Clouds Observed by ICESat and MODIS over Ice Sheets

As discussed in Section II, the atmospheric path delay strongly depends on cloud geometrical, optical and microphysical properties [2]. To achieve a realistic estimate of the magnitude of delays caused by clouds missed by the 1064 nm channel, the following parameters are needed as input to our radiative transfer model: cloud base height, cloud geometrical thickness, cloud optical depth, and cloud particle size and shape. Studies, such as [16], [17] and [18], have been conducted with ground-based measurements and *in-situ* measurements. *In-situ* and ground-based measurements are desirable in understanding polar cloud microphysics, but they are rare in the polar regions, especially in Antarctica. Space-borne lidars such as GLAS [14] and CALIOP (the Cloud-Aerosol Lidar with Orthogonal Polarization) [19] provide a unique collection of data, and studies with these data have provided new insight into polar cloud properties (e.g., [5], [8] and [20]).

In this study, the distributions of cloud base height and cloud optical depth are derived from the GLAS L2A campaign dataset. Because cloud geometrical thickness acts collaboratively with cloud base height, it is not treated as an independent variable. In the following calculations, we assume that clouds are 500 m thick. Cloud thickness distributions (not shown) calculated from GLAS L2A peak at around 500 m. Fig. 8a gives the 2-D histogram of cloud base height vs. cloud optical depth for $\tau \leq 0.2$. These clouds are the focus of this study, because they are the ones that the 1064 nm channel tends to miss.

In addition to cloud optical depth, cloud base height and cloud geometrical thickness, path delay simulations require the phase function of the cloud particles, or equivalently, particle size and shape. Ice cloud particles are a mixture of different habits and the determination of their phase functions is a complicated task [24]. Based on the ground-based observations around South Pole, Lawson et al. [17] reported that, of the all crystals observed, 30% were rosette shapes (mixed-habit rosettes, plate-like poly-crystals, and rosette shapes with side planes), 45% were diamond dust shapes (columns, thick plates, and plates), and 25% were irregular shapes. However, phase functions based on these observations are not readily available. In this study, we adopt the MODIS cirrus cloud microphysical model [12]. When the effective radius r_e is small (r_e < 35 μm), the habit mixture is prescribed as 50% bullet rosettes, 25% hexagonal plates and 25% hollow columns. When $r_e \geq 35\ \mu m$, the habit mixture is 30% aggregates, 30% bullet rosettes, 20% hexagonal plates, and 20% hollow columns. As shown in Fig. 8b, the MODIS retrieved particle effective radii vary from 10 μm to 50 μm. MODIS retrievals over the polar regions have certain limitations. Due to the strong shortwave reflectance and the low thermal brightness temperature of the surface, it is more difficult for passive remote sensing techniques to separate cloudy and cloud-free areas (e.g., [25] and [26]). Hence, the retrievals of cloud optical depth and particle effective radius over these regions may have large uncertainties [21].

VI. Estimated Path Delay over Ice Sheets

Based on the statistics presented in Section IV and V, we are able to estimate the path delay resulting from the clouds missed by the 1064 nm channel analysis as a function of telescope FOV. To do this, we calculate the average path delay as an integral:

$$I(\Delta\psi) = \iiint p_{missed}(\tau)\, p(\tau, h_b, r_e) L(\tau, h_b, r_e; \Delta\psi) d\tau dh_b dr_e \quad (2)$$

where $\Delta\psi$ is the telescope FOV; $p_{\text{missed}}(\tau)$ is the probability density function (pdf) of clouds with optical depth τ being missed by the 1064 nm channel due to the lower signal to noise ratio; $p(\tau,h_b,r_e)$ is the pdf of clouds with optical depth τ, base height h_b (relative to surface elevation), and particle effective radius r_e; and, $L(\tau,h_b,r_e;\Delta\psi)$ is the Monte Carlo calculated path delay as a function of $\Delta\psi$ for each combination of τ, r_e and h_b.

Even though there is a known correlation between ice particle size and cloud temperature [22], our analysis of thin polar clouds observed by GLAS and MODIS does not show any pronounced correlation between cloud base height, cloud optical depth and cloud particle effective radius (Fig. 8). As a first approximation, we can consider these three variables independent from each other. Thus Eq. (2) can be written as:

$$I(\Delta\psi) = \iiint p_1(\tau) p_2(h_b) p_3(r_e)\, L(\tau, h_b, r_e; \Delta\psi)\, d\tau dh_b dr_e \quad (3)$$

where $p_1(\tau) = p_{\text{missed}}(\tau)\ p(\tau)$ is the pdf of the clouds with optical depth τ undetected by the 1064 nm channel; $p_2(h_b)$ is the pdf of cloud base height h_b; $p_3(r_e)$ is the pdf of particle effective radius r_e.

The values of the distributions of cloud optical depth, cloud effective radius and cloud base height over Greenland and East Antarctica used in the calculation of average path delays are shown as Table 1. The results on the expected path delay caused by the missed clouds as a function of telescope field of view is displayed in Fig. 9. The error bars give the standard deviation of the path delay calculations for different cloud base heights, cloud optical depths and cloud particle effective radii. If the FOV is kept the same as the current ICESat, then over Greenland and East Antarctica, the bias would be 4.7±4.0 cm and 4.3±3.9 cm, respectively. Reducing the telescope FOV can significantly reduce the bias. If the FOV is reduced to 167 μrad, path delay will be around 0.9±0.7 cm over Greenland and 0.8±0.7 cm over East Antarctica.

We emphasize here four important points: 1) the above values of path delay are not weighted with the total number of surface elevation retrievals; 2) the fractions of undetected clouds are calculated based on the GLAS cloud optical depth product, which is 1 Hz, while surface elevation retrievals are

on a 40 Hz basis; 3) blowing snow is not accounted; and finally, 4) to investigate the impact of undetected clouds on the long-term trend of ice sheet elevation, we need to take into account the annual variability of the properties of the these clouds.

Let us briefly discuss the first two points. For simplicity, we assume that the total number of surface elevation retrievals is equal to the total number of clear pixels as determined by the 1064 nm channel. Then we can estimate the fraction of cloudy pixels misclassified as clear. Our calculations show that during the L2A campaign, the clear sky fractions over Greenland were 40% and 46% and, over East Antarctic 66% and 72%, for the 532 nm and 1064 nm channels, respectively. Hence the fraction of misclassified clouds is (46-40)/46=13% over Greenland and (72-66)/72=8% over East Antarctica. Calculations show similar results for smaller Antarctic regions, e.g., Pine Island, Lake Vostok and Interior West Antarctica. To summarize, roughly 10% of all laser shots identified by the 1064 nm channel as clear are actually misclassified cloudy shots that result in range delay. Thus our estimated average path delay due to undetected clouds has to be reduced by a factor of 10.

It is important to note that the above results are for the 1 Hz data. Since the 40 Hz data are used for surface elevation retrievals, we need to understand the 40 Hz range delay as well. In general, it is not a straightforward problem because the 532-nm channel does not provide retrievals of COD at 40 Hz. However, with some simplified assumptions range delay for 40 Hz can be estimated based on the 1 Hz estimates. If we assume constant signal, then averaging over 40 (independent) data points will increase the signal-to-noise ratio by a factor of $\sqrt{40} = 6.3$. If we further assume that for optically thin clouds the backscatter signal is proportional to COD, then the optically thicker clouds will be undetected at 40 Hz as likely as their 6.3 times thinner counterparts at 1 Hz. Next, since for thin clouds, the photon path delay and COD is approximately linearly related (see, Fig. 3), the average path delay would be also 6.3 times larger.

VII. Summary and Discussion

Duda et al. [2] showed that atmospheric path delay is sensitive to cloud height, cloud optical depth, ice particle phase functions, and the telescope FOV. This study complements [2] in three ways. (1) Atmospheric path delay due to thin clouds missed by the 1064 nm channel is determined using cloud observations by GLAS and MODIS. (2) The state-of-the-art models of scattering phase functions were used and the effect of cloud particle size and shape on atmospheric path delay has been studied. (3) Contributions to the path delay from different orders of scattering have been estimated. For very thin clouds missed by the 1064 nm channel, the single scattering approximation is found to be accurate enough and an analytical path delay model has been developed for this case. The major findings of this study can be summarized as follows.

Path delay is strongly affected by the forward scattering peak of the cloud particle phase function, or equivalently, the size and shape of the particles. However, the phase function effect substantially decreases with a reduction in the telescope FOV.

As a first-order approximation, atmospheric path delay can be calculated from a simple analytical formula. This formula, accounting for the delay caused by first order scattering photons, provides an efficient way to estimate the delay resulting from very thin clouds.

The 1064 nm channel alone tends to miss very thin clouds. According to the 1 Hz GLAS products, this channel fails to record about 20~30% of the transparent clouds. The majority of the undetected clouds have $\tau \le 0.2$.

Calculations of the expected path delay resulting from undetected clouds (so called, the residual bias) using GLAS and MODIS data show that reducing telescope FOV from 475 μrad (current ICESat) to 167 μrad (proposed for ICESat-II) will substantially mitigate the problem. The expected mean path delay due to undetected clouds for 167 μrad FOV and the 40 Hz data found to be smaller than 1 cm. However, since the ICESat-II orbit will follow a 91 day repeat cycle that provides only four measurements at a given point each year, the low rate of sampling requires accounting not only for the expected average bias but also for the maximum possible errors. In addition, the effect of blowing snow, which could potentially cause larger delay, is not considered in this study and will be reported separately.

Appendix

A Simple Analytical Model for Atmospheric Path Delay Caused by Single Scattering in Clouds

Here we derive a simple analytical model for atmospheric path delay caused by first order scattering. This model provides an efficient way to estimate path delays due to very thin clouds. A more complicated model that includes second order scattering will be investigated in a follow-up study.

From Fig. A1, for photons scattered at angle θ, the path delay can be calculated as [2]:

$$\Delta(z,\theta) = \frac{z}{\cos(\theta)} - z \tag{A1}$$

Let's only consider the range delay caused by photons experiencing single scattering, which could happen either on the downward path to surface or on the upward path to the sensor. The probability of photons being scattered once within a cloud of optical depth τ can be written as (see e.g., [23] p. 219):

$$p_1 = \tau e^{-\tau} \tag{A2}$$

Assuming a Lambertian surface with albedo α_s, the total

delay resulting from photons scattered once on the down/up path and un-scattered on the up/down path is:

$$[\tau e^{-\tau}(\frac{1}{2}\int_0^{\theta_s}\Delta(z,\theta)P(\theta)\sin(\theta)d\theta)]\alpha_s e^{-\tau} = \alpha_s \tau e^{-2\tau}(\frac{1}{2}\int_0^{\theta_s}\Delta(z,\theta)P(\theta)\sin(\theta)d\theta) \quad \text{(A3)}$$

where θ_s is the largest possible scattering angle for a photon to stay in the FOV and $P(\theta)$ is the scattering phase function normalized as:

$$\frac{1}{2}\int_0^{\pi} P(\theta)\sin(\theta)d\theta = 1 \quad \text{(A4)}$$

Given satellite orbital altitude h (in meters), cloud height z (in meters) and telescope FOV f (in μrad), θ_s can be calculated as following:

$$\theta_s = \arctan(\frac{f \times 10^{-6} \times h}{2z}) \quad \text{(A5)}$$

The probability of photons reaching the sensor without being scattered within the cloud is:

$$S_0 = \alpha_s e^{-2\tau} \quad \text{(A6)}$$

The probability of photons reaching the sensor being scattered once within the cloud is:

$$S_1 = 2\alpha_s \tau e^{-2\tau}(\frac{1}{2}\int_0^{\theta_s} P(\theta)\sin(\theta)d\theta) \quad \text{(A7)}$$

Hence the average delay caused by the photons being scattered once can be calculated as:

$$\overline{\Delta} = \frac{2\alpha_s \tau e^{-2\tau}(\frac{1}{2}\int_0^{\theta_s}\Delta(z,\theta)P(\theta)\sin(\theta)d\theta)}{\alpha_s e^{-2\tau} + 2\alpha_s \tau e^{-2\tau}(\frac{1}{2}\int_0^{\theta_s} P(\theta)\sin(\theta)d\theta)} = \frac{\tau(\int_0^{\theta_s}\Delta(z,\theta)P(\theta)\sin(\theta)d\theta)}{1+\tau(\int_0^{\theta_s} P(\theta)\sin(\theta)d\theta)} \quad \text{(A8)}$$

If only zero and first order scattering are considered, then the contribution of zero order scattering to lidar return is:

$$p_{s_0} = \frac{\alpha_s e^{-2\tau}}{\alpha_s e^{-2\tau} + 2\alpha_s \tau e^{-2\tau}(\frac{1}{2}\int_0^{\theta_s} P(\theta)\sin(\theta)d\theta)} = \frac{1}{1+2\tau(\frac{1}{2}\int_0^{\theta_s} P(\theta)\sin(\theta)d\theta)} \quad \text{(A9)}$$

As shown in Fig. 4a, the probability of photons being scattered into the forward scattering angle range [0, θ_s], $\frac{1}{2}\int_0^{\theta_s} P(\theta)\sin(\theta)d\theta$, is about 50% for a variety of particle sizes and shapes. Approximately, the contribution of zero order scattering can be written as:

$$p_{s_0} \approx \frac{1}{1+\tau} \times 100\% \quad \text{(A10)}$$

Similarly, the contribution of the first order scattering can be written as:

$$p_{s_1} = (1 - \frac{1}{1+\tau}) \times 100\% = \frac{\tau}{1+\tau} \times 100\% \quad \text{(A11)}$$

Figure A2 shows the comparison between the results of this analytical model and our 3-D Monte Carlo model when only single scattering is taken into account. As can be seen from the figure, these results are essentially identical.

ACKNOWLEDGMENT

The authors would like to thank Drs. Christine Chiu, Stephen Palm, James Spinhirne, and Zhibo Zhang for helpful discussions and advice. We also appreciate the helpful comments and suggestions from two anonymous reviewers. This work was supported by the National Aeronautics and Space Administration's ICESat II Science Definition Project.

REFERENCES

[1] Zwally H.J., B. Schutz, W. Abdalati,J. Abshire, C. Bentley, A. Brenner, J. Bufton, J. Dezio, D. Hancock, D. Harding, T. Herring, B. Minster, K. Quinn, S. Palm, J. Spinhirne, and R. Thomas, "ICESat 's laser measurements of polar ice, atmosphere, ocean, and land," *J. Geodynamics*, vo. 34, pp. 405–445, 2002.

[2] Duda, D.P., J. D. Spinhirne, and E.W. Eloranta, "Atmospheric multiple scattering effects on GLAS altimetry – part I: Calculations of single path bias," *IEEE Trans. Geos. Rem. Sens.*, vol. 39, pp. 92-101, 2001.

[3] Eloranta, E. W., "A practical model for lidar multiple scattering," *Appl. Opt*., vol. 37, pp. 2464–2472, 1998.

[4] Mahesh, A., J. D. Spinhirne, D.P. Duda, and E.W. Eloranta, "Atmospheric multiple scattering effects on GLAS altimetry – part II: Analysis of expected errors in Antarctic altitude measurements," *IEEE Trans. Geos. Rem. Sens.*, vol. 40, pp. 2353-2362, 2002.

[5] Spinhirne, J.D., S.P. Palm, W.D. Hart, D.L. Hlavka, and E.J. Welton, "Cloud and aerosol measurements from GLAS: Overview and initial results," *Geophys. Res. Letters*, Vol. 32 (22), L22S03, doi:10.1029/2005GL023507, 2005

[6] Yang, Y., A. Marshak, J. C. Chiu, W. J. Wiscombe, S. P. Palm, A. B. Davis, D. A. Spangenberg, L. Nguyen, J. D. Spinhirne, and P. Minnis, "Retrievals of Thick Cloud Optical Depth from the Geoscience Laser Altimeter System (GLAS) by Calibration of Solar Background Signal," *J. Atmos. Sci*., vol. 65, pp. 3513–3527, 2008.

[7] National Research Council, "*Earth Science and Applications from Space: National Imperatives for the Next Decade and Beyond*," prepared by the Committee on Earth Science and Applications from Space: A Community Assessment and Strategy for the Future, National Research Council, National Academies Press, 2007.

[8] Spinhirne, J.D., S.P. Palm, and W.D. Hart, "Antarctica cloud cover for October 2003 from GLAS satellite lidar profiling," *Geophys. Res. Letters*, vol. 32, L22S05, doi:10.1029/2005GL023782, 2005.

[9] Cahalan, R. F., M. McGill, J. Kolasinski, T. Várnai, and K. Yetzer, "THOR – Cloud Thickness from Offbeam Lidar Returns," *J. Atmos. Ocean. Tech.*, vol. 22, pp. 605-627, 2004.

[10] Cahalan R. F. et al., "The International Intercomparison of 3D Radiation Codes (I3RC): Bringing together the most advanced radiative transfer tools for cloudy atmospheres," *Bulletin Amer. Meteor. Soc. (BAMS),* vol. 86, pp. 1275-1293, 2005.

[11] Abdalati, W. et al., "Report of the As-hoc Science Definition team for the Ice Cloud and Land Elevation Satellite-II (ICESat-II)," Report can be found at https://cires.colorado.edu/~waleed/, 2008.
[12] Baum, B. A., P. Yang, A. J. Heymsfield, S. Platnick, M. D. King, Y. X. Hu, and S. T. Bedka, "Bulk Scattering Properties for the Remote Sensing of Ice Clouds. Part II: Narrowband Models," *J Appl. Meteor*., vol. 44, pp. 1896-1911, 2005.
[13] Yang, P., H. Wei, H.-L. Huang, B. A. Baum, Y. X. Hu, G. W. Kattawar, M. I. Mishchenko, and Q. Fu, "Scattering and absorption property database for nonspherical ice particles in the near- through far-infrared spectral region," *Appl. Opt.*, vol. 44, pp. 5512-5523, 2005.
[14] Palm, S. P., J. D. Spinhirne, W. D. Hart, and D. L. Hlavka, "GLAS atmospheric data products, algorithm theoretical basis document, version 4.2," GSFC, Greenbelt, Md. (Available at: http://www.csr.utexas.edu/glas/pdf/glasatmos.atbdv4.2.pdf.), 2002.
[15] Zwally, H.J., M.A. Beckley, A.C. Brenner and M.B. Giovinetto, "Motion of major ice-shelf fronts in Antarctica from slantrange analysis of radar altimeter data, 1978–98," *Ann. Glaciol.*, vol. 34, pp. 255–262, 2002.
[16] Mahesh, A., von P. Walden, and S. G. Warren, "Ground-based infrared remote sensing of cloud properties over Antarctic Plateau. Part II: Cloud optical depths and particle sizes," *J. Appl. Meteo.*, vol. 40, 1279-1294, 2001.
[17] Mitchell, D.L. and R.P. d'Entremont, "Satellite Remote Sensing of Small Ice Crystal Concentrations in Cirrus Clouds," *Proc. ICCP Cancun Mexico*, pp. 7-11, 2008.
[18] Lawson, R.P., B.A. Baker, P. Zmarzly, D. O'Connor, Q. Mo, J.-F. Gayet, and V. Shcherbakov, "Microphysical and optical properties of ice crystals at South Pole Station," *J. Appl. Meteor. Climatol*, vol. 45, 1505-1524, 2006.
[19] Vaughan, M., S. Young, D. Winker, K. Powell, A. Omar, Z. Liu, Y. Hu, and C. Hostetler, "Fully automated analysis of space-based lidar data: an overview of the CALIPSO retrieval algorithms and data products," *Proc. SPIE*, 5575, pp. 16-30, 2004.
[20] Weisz, E., J. Li, W. P. Menzel, A. K. Heidinger, B. H. Kahn, and C.-Y. Liu, "Comparison of AIRS, MODIS, CloudSat and CALIPSO cloud top height retrievals," *Geophys. Res. Lett.*, vol. 34, L17811, doi:10.1029/2007GL030676, 2007.
[21] Pavolonis, M. J., and J. R. Key, "Antarctic cloud radiative forcing at the surface estimated from the AVHRR Polar Pathfinder and ISCCP D1 datasets, 1985-93," *J. Appl. Meteorol.*, vol. 42, pp. 827–840, 2003.
[22] Heymsfield, A., "Properties of tropical and midlatitude ice cloud particles ensembles. Part II: Applications for mesoscale and climate models," *J. Atmos. Sci.*, vol. 60, pp. 2592–2611, 2003.
[23] Thomas, G. E., and K. Stamnes, 1999: Radiative transfer in the atmosphere and ocean. Cambridge University Press, 517 pp, 1999.
[24] Yang, P., G. W. Kattawar, G. Hong, P. Minnis, and Y. Hu, "Uncertainties with the surface of ice particles in satellite-based retrieval of cirrus clouds: Part I. Single-scattering properties of ice crystals with surface roughness," *IEEE Trans. Geosci. Remote Sens.*, vol. 46, 1940-1947, 2008.
[25] Mahesh, A., M. A. Gray, S. P. Palm, W. D. Hart, and J. D. Spinhirne, "Passive and active detection of clouds: Comparisons between MODIS and GLAS observations," *Geophys. Res. Lett.*, vol. 31, L04108, doi:10.1029/2003GL018859, 2004.
[26] Naud, C., J.-P. Muller, and P. de Valk, "On the use of ICESAT-GLAS measurements for MODIS and SEVIRI cloud-top height accuracy assessment," *Geophys. Res. Lett.*, vol. 32, L19815, doi:10.1029/2005GL023275, 2005.

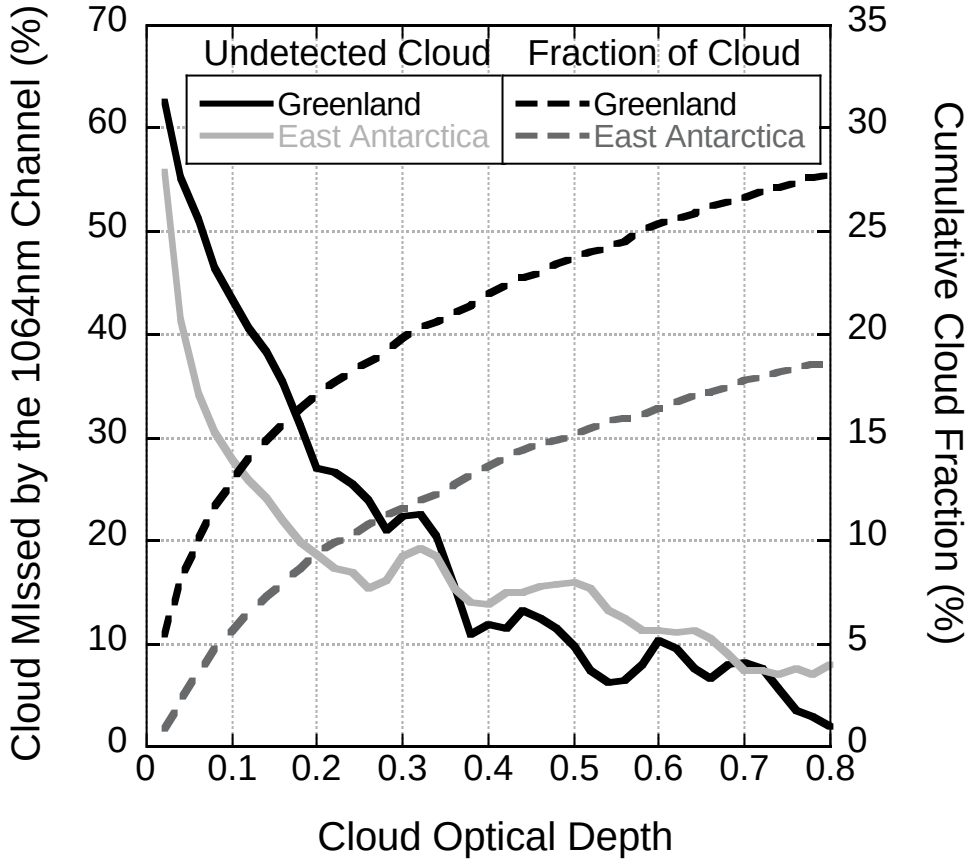

Fig. 1. The probability of a cloud being missed by the 1064 nm channel when compared to the cloud detection results of the 532 nm channel as a function of cloud optical depth (COD) and the cumulative cloud fraction, as detected by the 532 nm channel for Greenland and East Antarctica. Fraction of cloud with a given optical depth is defined as the frequency of occurrence of clouds out of the total number of observations. Data are the 1 Hz product from the GLAS L2A campaign (25 September to 19 November 2003).

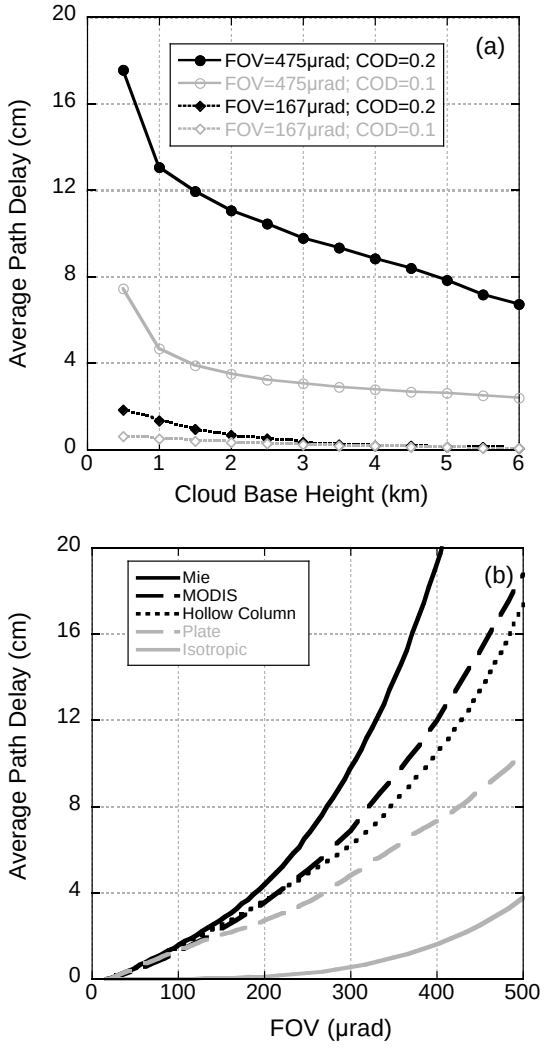

Fig. 2. Examples of parameters affecting atmospheric path delay. (a) Path delay as a function of cloud base height for clouds of two different optical depths (0.1 and 0.2), and two different field-of-views (167 μrad and 475 μrad). Cloud geometrical thickness is 500 m. MODIS ice phase function for r_e = 20 μm used. (b) Path delay as a function of the telescope FOV for different particle shapes. Cloud base height is 500 m; cloud geometrical thickness is 500 m; τ = 0.2; r_e = 20 μm. Isotropic phase function is added for illustrative purposes.

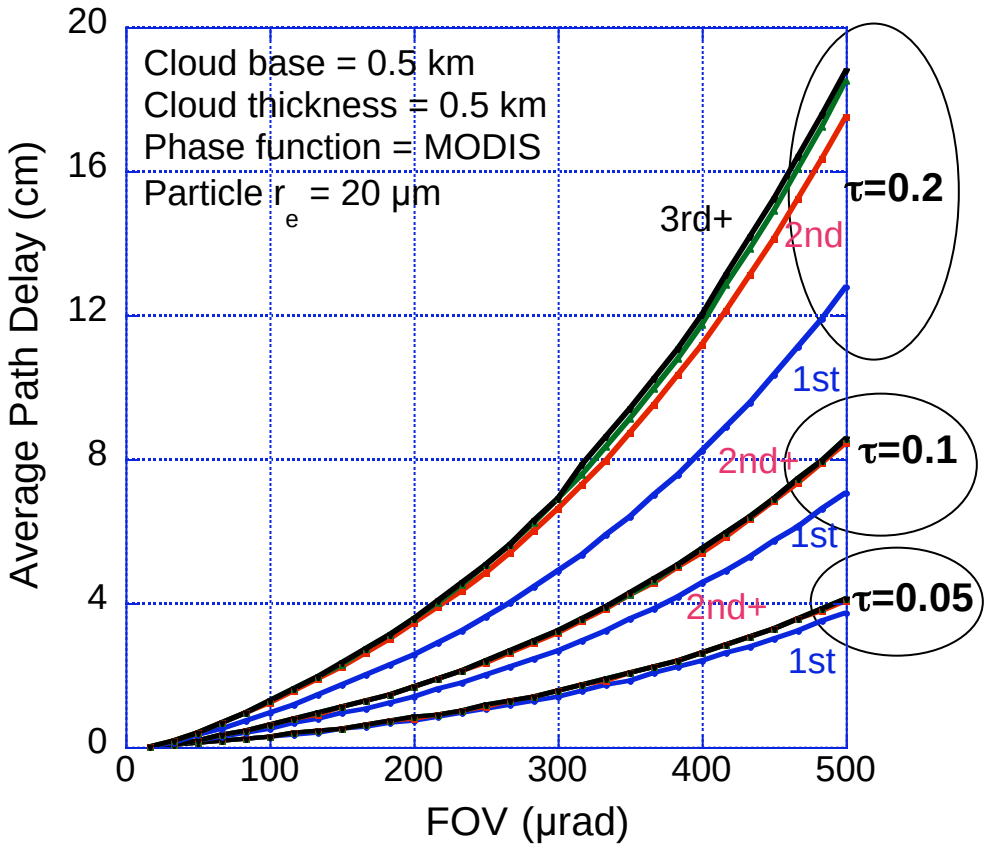

Fig. 3. Path delay contributions from different orders of scattering as a function of FOV: for τ = 0.05, 0.1 and 0.2; cloud at 0.5 - 1.0 km; r_e = 20 μm; MODIS ice phase function used. Blue, red, green and black lines illustrate cases when up to 1st , 2nd, 3rd, and all orders of scattering are taken into account, respectively.

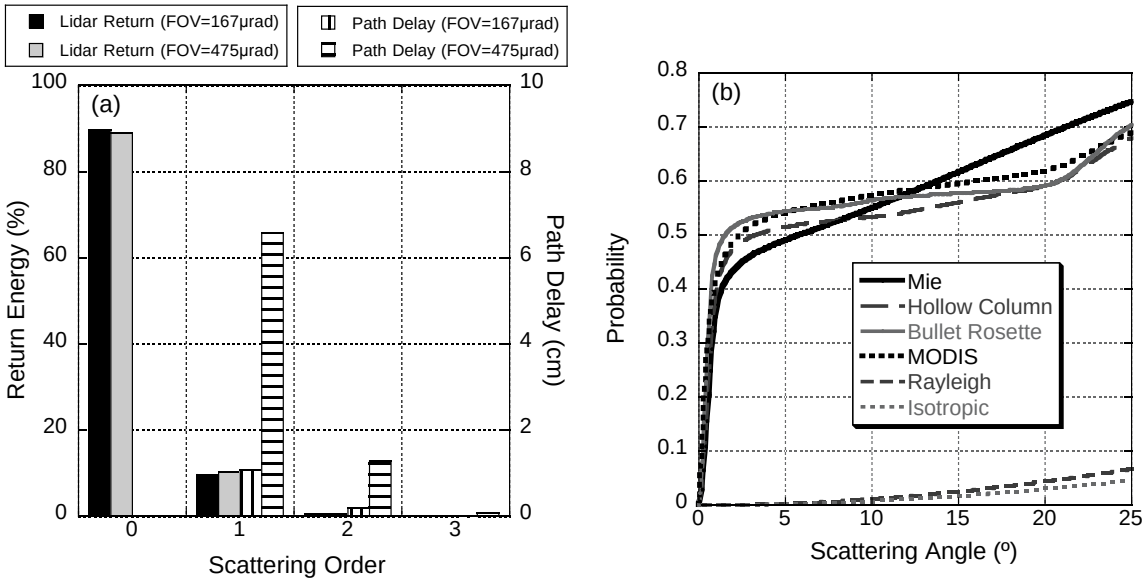

Fig. 4. (a) Monte Carlo simulated results of contributions to both lidar return and path delay from different orders of scattering for two FOVs: 475 μrad and 167 μrad with cloud optical depth 0.1. Cloud base height is 500 m; cloud geometrical thickness is 1000 m; MODIS phase function used; r_e = 20 μm. (b) Phase function integrals of different particle shapes, which give the probability of photons being scattered within the scattering angle. Phase functions of Mie, Hollow Column, Bullet Rosette, and MODIS are for r_e = 20 μm. Rayleigh and isotropic phase functions are included for illustrative purposes.

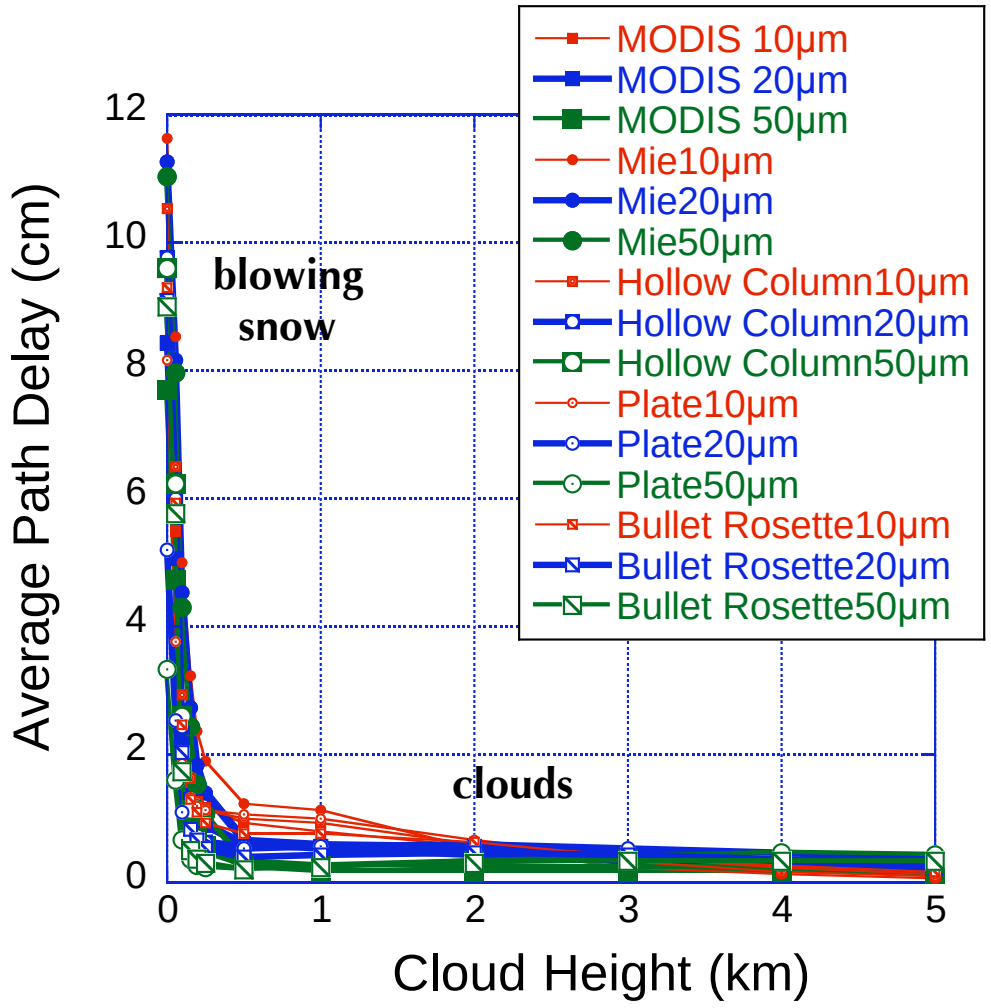

Fig. 5. Path delay as a function of scattering layer altitude and particle shape for cloud optical depths of 0.05. FOV = 167 μrad. Calculated with the analytical model presented in the Appendix.

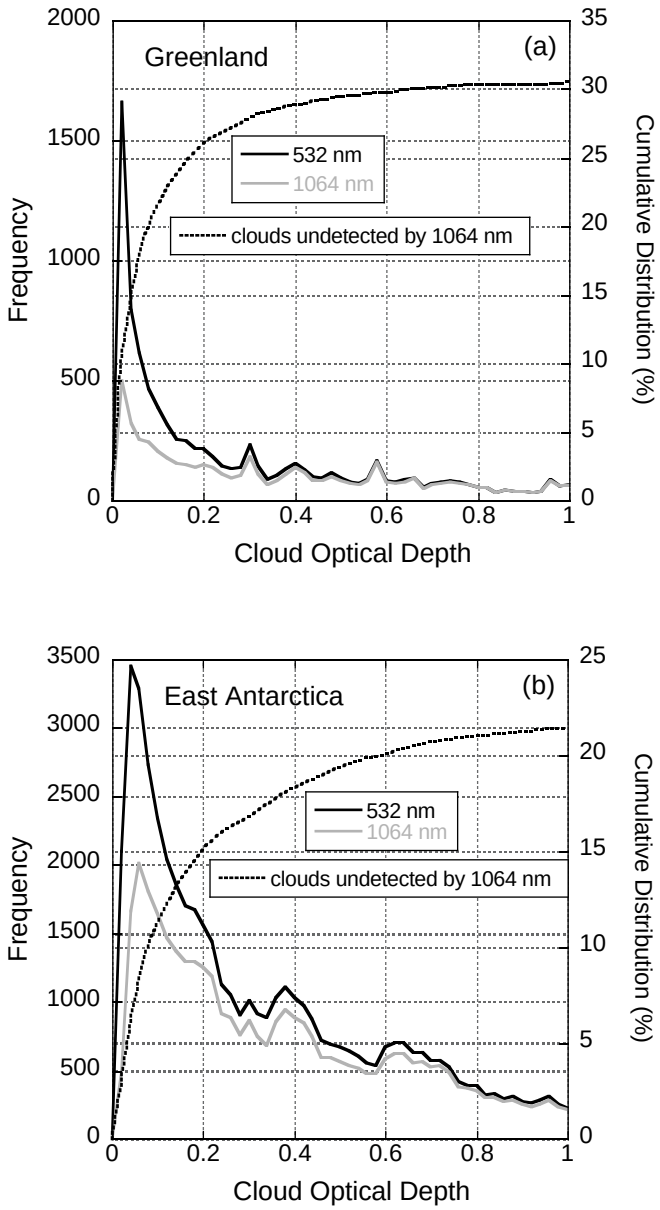

Fig. 6. The frequency of cloud optical depth retrieved from the GLAS 532 nm channel (black line) together with clouds detected by the 1064 nm channel (grey line); the dotted line is the cumulative distribution of thin clouds missed by the 1064 nm channel, defined as the frequency of missed clouds out of all transparent clouds detected by the 532 nm channel. Transparent clouds are clouds thin enough for GLAS to have ground return. Based on the 1 Hz data of GLAS L2A campaign for (a) Greenland; (b) East Antarctica (compare with Fig. 4 in [5]).

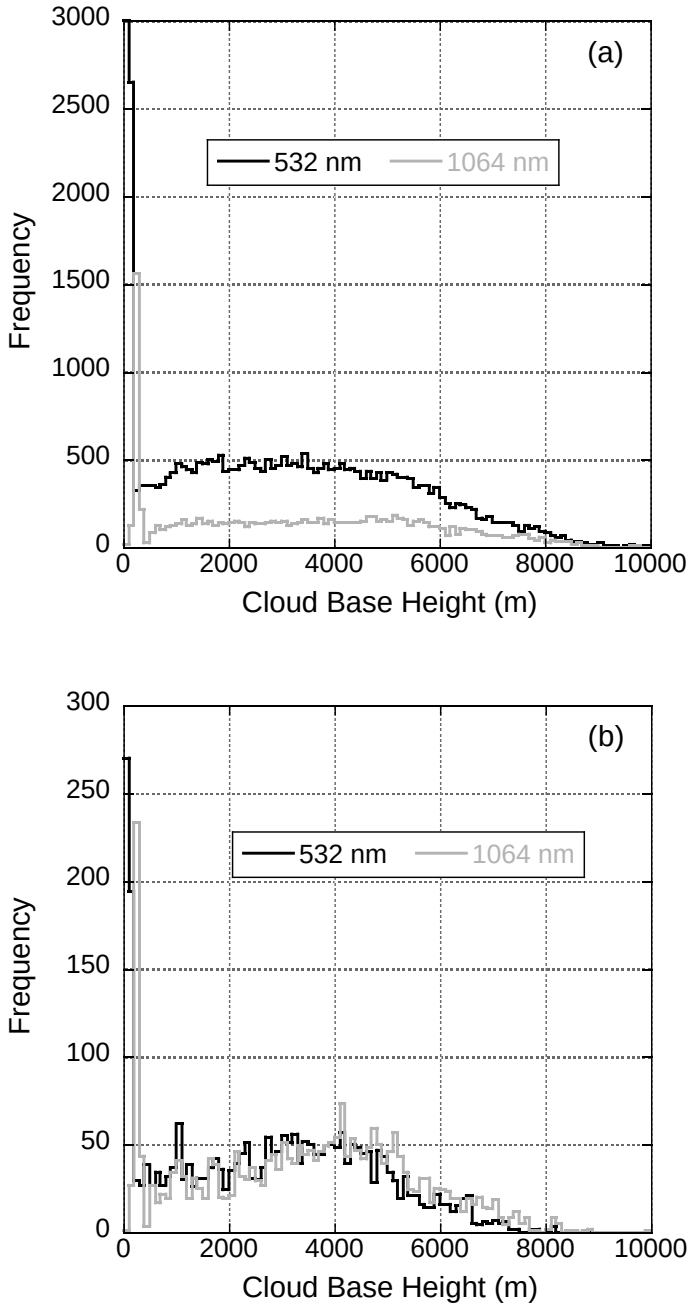

Fig. 7. The frequency of cloud base height retrieved from the GLAS 532 nm channel (black line) and the 1064 nm channel (grey line). Based on the GLAS L2A campaign for East Antarctica for clouds with (a) $\tau \leq 0.2$ and (b) $1.0 \leq \tau \leq 2.0$.

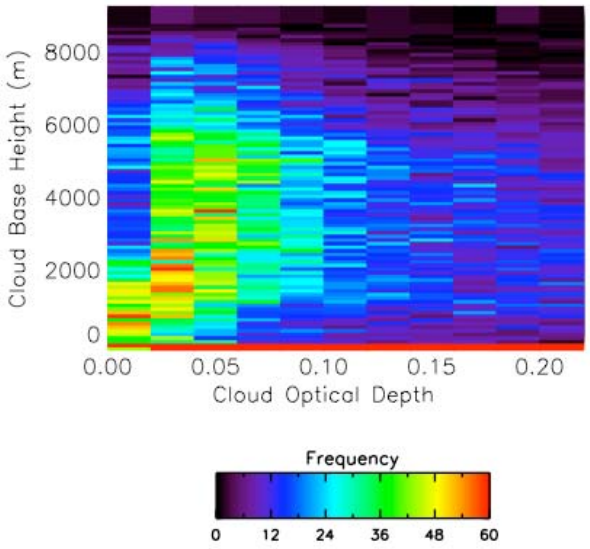

(a)

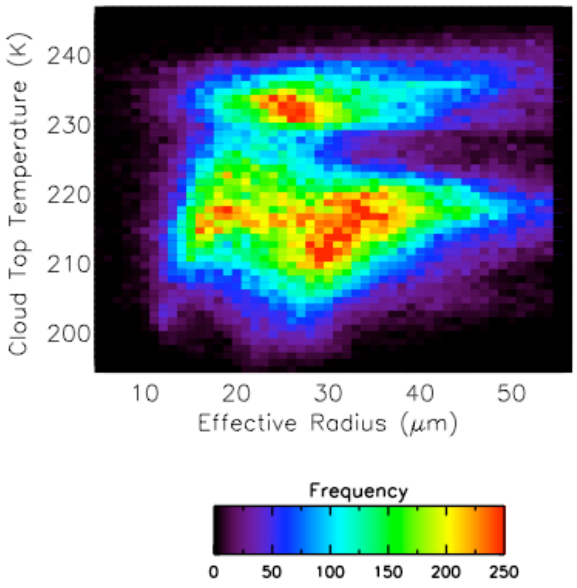

(b)

Fig. 8. Two-dimensional histograms for (a) GLAS COD vs. cloud base height for clouds with $\tau \leq 0.2$ over East Antarctica. Data are from the GLAS L2A campaign. (b) MODIS cloud top temperature vs. ice particle effective radius over East Antarctica. Data are from MODIS Aqua and Terra for the fall of 2003 (the time period as for the GLAS L2A campaign).

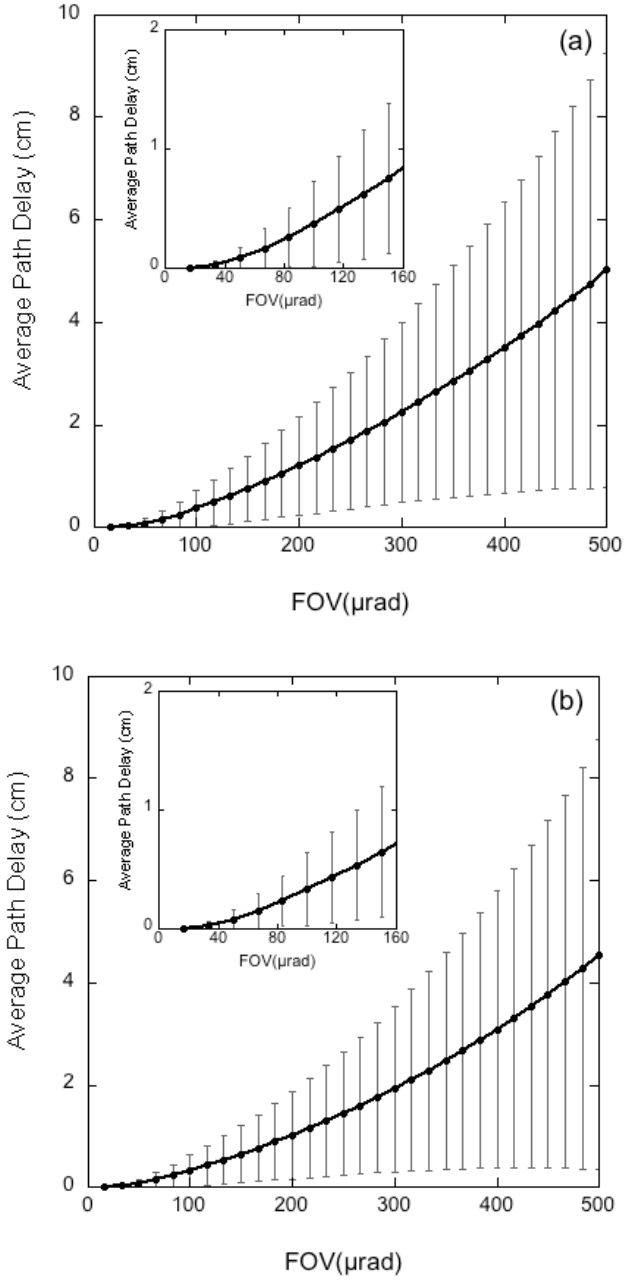

Fig. 9. Estimated average path delay resulting from clouds missed by the 1064 nm channel for 1Hz data. Blowing snow is not included. (a) Greenland; (b) East Antarctica. Insets are the zoomed-in version for smaller FOVs.

Appendix Figures

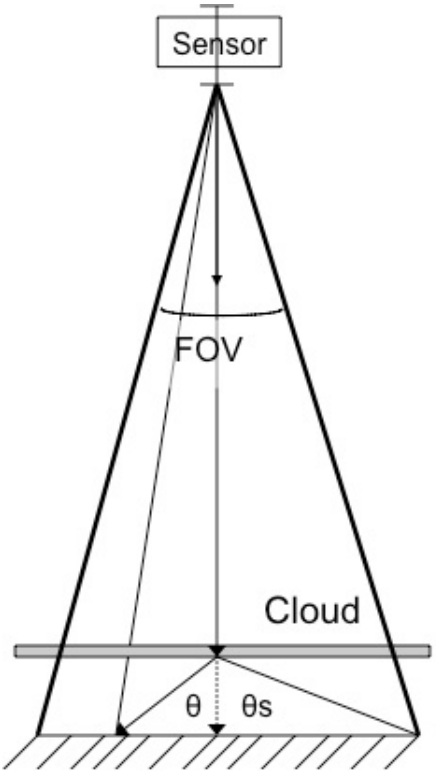

Fig. A1. A schematic picture of path delay caused by forward scattering. Solid arrow lines represent the path of scattered photons. Dashed arrow line represents the path of non-scattered photons. θ is the scattering angle and θ_s is the largest possible scattering angle for a photon to stay in the FOV.

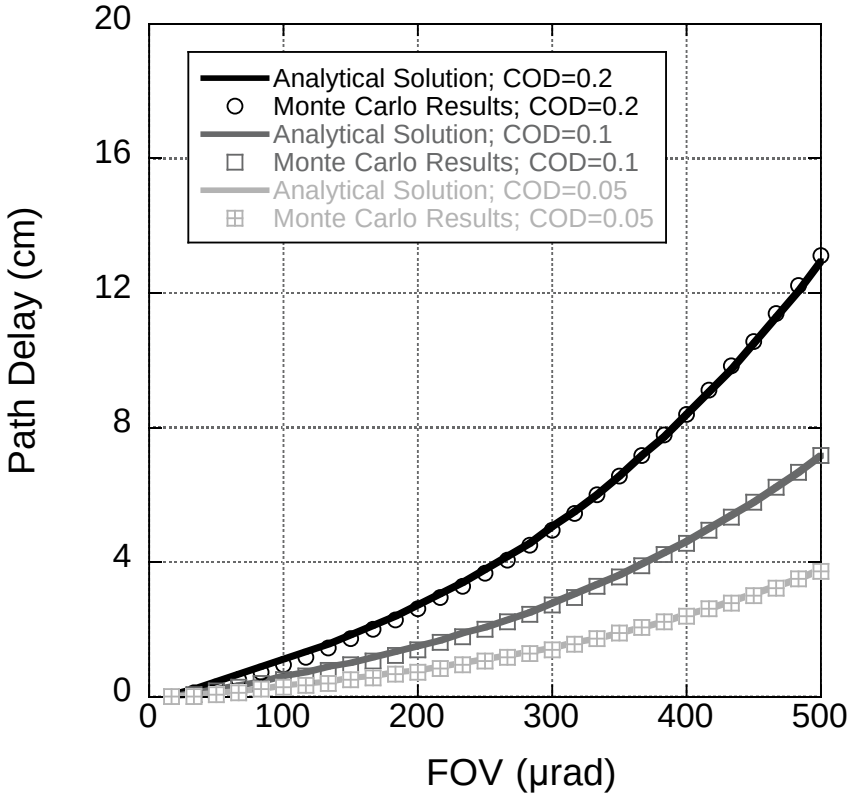

Fig. A2. Comparison of results from the analytical model and the Monte Carlo model with only single scattering. Clouds at 500 m to 1000 m. MODIS phase function for r_e = 20 μm used.

Table 1: Probability density function of clouds potentially missed by the 1064 nm channel used in estimating average path delays over Greenland and Antarctica. In the table, EA stands for East Antarctica and GL stands for Greenland.

Cloud Optical Depth			Effective Radius			Cloud Base Height		
Value	PDF GL	PDF EA	Value (μm)	PDF GL	PDF EA	Value (m)	PDF GL	PDF EA
0.05	0.45	0.39	10	0.19	0.07	500	0.17	0.19
0.1	0.24	0.25	20	0.61	0.31	1000	0.20	0.21
0.15	0.15	0.17	30	0.15	0.32	2000	0.23	0.22
0.2	0.1	0.11	40	0.04	0.20	3000	0.21	0.19
0.25	0.06	0.08	50	0.01	0.10	4000	0.19	0.19